Journal of Sound and Vibration 329 (2010) 3856–3865

Contents lists available at ScienceDirect

Journal of Sound and Vibration

journal homepage: www.elsevier.com/locate/jsvi

Elastic stability of columns on partial elastic foundations under subtangential loading

Allan Struthers [a,*], Gopal Jayaraman [b]

[a] Mathematical Sciences, Michigan Technological University, 1400 Townsend Drive, Houghton, MI 49931, USA
[b] Mechanical Engineering, Michigan Technological University, USA

ARTICLE INFO

Article history:
Received 31 December 2009
Accepted 6 March 2010
Handling Editor: S. Ilanko
Available online 22 April 2010

ABSTRACT

Divergence and flutter instability of a cantilevered beam on a partial elastic foundation subjected to a subtangential load at the free end are investigated. The dependence of divergence and flutter critical loads on the tangency coefficient is studied parametrically to illustrate the effects of the extent, position, and modulus of the partial foundation. Particular attention is paid to the stabilizing and destabilizing effects of the various parameters.

1. Introduction

Divergence elastic instability of axially compressed columns with conservative loads on full and partial elastic foundations is examined in numerous [1–8] analytical and experimental papers. These studies show that increasing the foundation modulus (or foundation coverage) increases the minimum critical load for divergence.

Smith and Herrmann [9] showed that flutter complicates the situation for subtangential (described by the *tangency-coefficient* η which interpolates between conservative $\eta=0$ and follower $\eta=1$) loads. Specifically, [9] shows that a uniform elastic foundation has no effect on the stability of a uniform column subject to a non-conservative load with $\eta>0.5$ by establishing that flutter is the governing instability for $\eta>0.5$ and that (for any value of η) the flutter critical load is independent of the foundation modulus. This surprising and counter intuitive result generated a flurry of activity: Sundarajan [10] extended the result to fully supported columns with geometrically similar foundation modulus and mass distributions: Jacoby and Elishakoff [11] incorporated discrete mass and foundation distributions in Sundarajan's results; Elishakoff and Jacoby [12] used simple model structures to clarify the counter-intuitive behavior; while Rao and Rao [13] examined $\eta=0.1,0.2,\ldots,0.9,1.0$ and showed that flutter was the governing instability for stiffer foundations with $\eta\geq 0.4$ and numerically verified that the critical flutter load was independent of the foundation modulus for those η values.

Recently, Kirillov and Seyaranien [14] gave a complete analytical solution of the Smith–Herrmann problem for $0\leq\eta\leq 1$ demonstrating that as the foundation modulus increases the critical divergence load increases with one end in contact with constant flutter domain.

Hauger and Vetter [15] demonstrated that a non-uniform foundation can destabilize a column with respect to flutter. Specifically, [15] shows that (for a particular quadratic variation of the foundation modulus and follower $\eta=1$ loading) a two-term Galerkin approximation to the critical flutter load decreases as the foundation modulus increases. This

* Corresponding author.
E-mail address: struther@mtu.edu (A. Struthers).

0022-460X/$ - see front matter © 2010 Elsevier Ltd. All rights reserved.
doi:10.1016/j.jsv.2010.03.004

anomalous behavior prompted studies describing other situations where a foundation decreases the flutter stability of a structure. Lee and Young [16] showed (using transfer matrices) that (for a sufficiently stiff foundation with follower load) tapering a column increases the flutter critical load. Elishakoff and Wang [17] showed (using an algebraically involved, two-term, Galerkin approximation) that a partial foundation can reduce the critical flutter load for a uniform column subject to a follower load. Kirillov and Seyranian [14] computed (with a variational argument) the analytical derivative of the flutter load with respect to positive perturbations (located at position x on the column) from a uniform foundation modulus. The derivative is positive for some η and x and negative for others demonstrating conclusively that non-uniform foundations can stabilize or destabilize the column under non-conservative loads.

There has been some controversy concerning the practical significance of follower/subtangential loads for physical structures. A letter to the editor of JSV by Koiter [18] claimed that there was no physical mechanism for experimental follower loads. The resulting discussion (a brief letter from Sugiyama et al. [19] followed by a substantial review article by Langthjem and Sugiyama [20]) stressed experimental observations of flutter instabilities and other physical situations (strikingly the stabilization of a flexible column by a compressive rocket) where observed physical behavior is best understood and modelled by subtangential loads. The editorial response [18] was to encourage discussion and reiterate to authors and referees the primary importance of physical relevance.

Subtangential loads (from solid–fluid interactions, etc.) are clearly potentially significant for light weight composite structures. Moreover, not all physical structures are engineered and two recent biomechanical models focus on follower loads and elastic foundations to explain the load carrying capabilities of the human spine and mosquito fascicle (biting structure).

The mosquito fascicle is a thin hollow needle with a surrounding structure (labium) that retracts as the fascicle penetrates the skin of the prey. Ramasubramanian et al. [21] model the fascicle as a variable length slender column on an elastic foundation with a subtangential load (actively applied by the mosquito's head) driving the fascicle into the skin. The assumption of subtangential loading is motivated by high speed video of the head motions of a mosquito feeding. The conclusions are that subtangential loading is helpful and that the support provided by the elastic foundation (labium) at the free end is essential for the mosquito to penetrate the skin.

The human spine is a slender flexible column with additional muscular and skeletal structures. The mechanical role that these additional structures play in supporting physiological loads has been investigated using a variety of tools. Andriacchi et al. [22] investigated the role of the skeletal components with a multi-component (39 physiologically accurate rigid-bodies representing vertebrae, ribs, etc. coupled by over 250 springs and beams representing soft tissue) spinal model and showed that the rib-cage (attached at the free end of the lumbar spine) significantly stiffened the spine. Patwardhan et al. [23] investigated the mechanical role of the musculature by attaching a cable system (to ensure that compressive loads followed the spinal curve) to cadaver spines and showed that although this structure failed under a 100 Newton vertical (Conservative) load it could sustain up to a physiologically realistic 1200 Newton follower load. Kim et al. [24] demonstrated that a finite element beam model for the spine with an active musculature (117 muscle pairs with physiological attachment points and load limits which constrain compressive loads in the beam to follow the spinal curve) could support physiological loads.

The simplest model problem (after removing physiological details) for both the fascicle and spine is a slender column on a partial elastic foundation under subtangential loading. In this paper, we bridge and extend the studies by Rao and Rao [13], Elishakoff and Wang [17], and Kirillov and Seyranian [14] to study the stability of the column in Fig. 1. The column is built-in at $x=0$ with a general subtangential load P at the free end $x=L$. A partial elastic foundation (the shaded region) extends from $\lambda_1 L$ to $\lambda_2 L$. We use the scaled length ($a=(\lambda_2-\lambda_1)$ and position $b=(\lambda_1+\lambda_2)/2$) of the partial foundation in our discussion of the results. The complete physical ranges $0\le\eta\le1$ and $0\le\lambda_1\le\lambda_2\le1$ are examined using an analytical technique (similar to that developed for an orthotropic plate problem by Jayaraman and Struthers [25]) to compute detailed information about the dependence of divergence and flutter critical loads on foundation modulus k, extent a and position b, as well as the tangency coefficient η. Elisahkoff and Wang [17] consider only follower ($\eta=1$) loads with foundation extending from the built in end ($\lambda_1=0$ or equivalently $a=2b$): we compare our analytical results to the results from their numerical approximation for $\lambda_1=0$ and $\lambda_2=1$. Rao and Rao [13] and Kirillov and Seyranian [14] consider the fully supported case ($\lambda_1=0$ and $\lambda_2=1$ or equivalently $a=1$ and $b=0.5$) for $\eta=0.1,0.2,\ldots,1.0$.

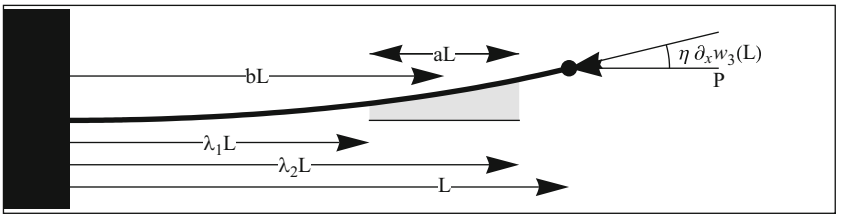

Fig. 1. Beam geometry and loading. The foundation (shaded portion) of length aL centered at bL extends from $\lambda_1 L$ to $\lambda_2 L$.

2. Problem formulation

We extend the notation and development of Elishakoff and Wang [17] to the column shown in Fig. 1. The column (with uniform mass density m and flexural rigidity EI) occupies the interval $0 \le x \le L$. It is built in at x=0 and subject to a subtangential follower force (with tangency coefficient $0 \le \eta \le 1$) P at the free end x=L. A uniform elastic foundation (with foundation modulus K) supports the central portion $x_1 = \lambda_1 L \le x \le \lambda_2 L = x_2$ of the column. The Bernoulli–Euler equations [17] for the lateral displacement w on the three regions (with EI the flexural rigidity, m the mass density per unit length, and K the foundation modulus) are

$$\begin{aligned}
&\mathrm{EI}\partial_{xxxx}w_1 + P\partial_{xx}w_1 + 0w_1 + m\partial_{tt}w_1 = 0, \quad 0 \le x < \lambda_1 L,\\
&\mathrm{EI}\partial_{xxxx}w_2 + P\partial_{xx}w_2 + Kw_2 + m\partial_{tt}w_2 = 0, \quad \lambda_1 L \le x < \lambda_2 L,\\
&\mathrm{EI}\partial_{xxxx}w_3 + P\partial_{xx}w_3 + 0w_3 + m\partial_{tt}w_3 = 0, \quad \lambda_2 L \le x < L.
\end{aligned} \tag{1}$$

The boundary (at the built-in end (x=0) and the free end (x=L)) and continuity (at the foundation transitions x=x_1 and x_2) conditions are

$$\begin{aligned}
&w_1(0,t) = 0, \quad \partial_{xx}w_3(L,t) = 0,\\
&\partial_x w_1(0,t) = 0, \quad \partial_{xxx}w_3(L,t) = \frac{P}{\mathrm{EI}}(\eta - 1)\partial_x w_3(L,t),\\
&w_1(x_1,t) = w_2(x_1,t), \quad w_2(x_2,t) = w_3(x_2,t),\\
&\partial_x w_1(x_1,t) = \partial_x w_2(x_1,t), \quad \partial_x w_2(x_2,t) = \partial_x w_3(x_2,t),\\
&\partial_{xx} w_1(x_1,t) = \partial_{xx} w_2(x_1,t), \quad \partial_{xx} w_2(x_2,t) = \partial_{xx} w_3(x_2,t),\\
&\partial_{xxx} w_1(x_1,t) = \partial_{xxx} w_2(x_1,t), \quad \partial_{xxx} w_2(x_2,t) = \partial_{xxx} w_3(x_2,t).
\end{aligned} \tag{2}$$

Substituting the modal forms $w_j(x,t) = \psi_j(x/L)\mathrm{e}^{\mathrm{i}\omega t}$ for j=1,2,3 into Eqs. (1) and (2) gives the three ordinary differential equations (ODE) for the displacement

$$\begin{aligned}
&\psi_1''''(\zeta) + F\psi_1''(\zeta) + (0 - \alpha^2)\psi_1(\zeta) = 0 \quad \text{for } 0 < \zeta < \lambda_1,\\
&\psi_2''''(\zeta) + F\psi_2''(\zeta) + (k - \alpha^2)\psi_2(\zeta) = 0 \quad \text{for } \lambda_1 < \zeta < \lambda_2,\\
&\psi_3''''(\zeta) + F\psi_3''(\zeta) + (0 - \alpha^2)\psi_3(\zeta) = 0 \quad \text{for } \lambda_2 < \zeta < 1,
\end{aligned} \tag{3}$$

along with the four boundary conditions and eight continuity conditions

$$\begin{aligned}
&\psi_1(0) = 0, \quad \psi_1(\lambda_1) = \psi_2(\lambda_1), \quad \psi_2(\lambda_2) = \psi_3(\lambda_2),\\
&\psi_1'(0) = 0, \quad \psi_1'(\lambda_1) = \psi_2'(\lambda_1), \quad \psi_2'(\lambda_2) = \psi_3'(\lambda_2),\\
&\psi_3''(1) = 0, \quad \psi_1''(\lambda_1) = \psi_2''(\lambda_1), \quad \psi_2''(\lambda_2) = \psi_3''(\lambda_2),\\
&\psi_3'''(1) = F(\eta - 1)\psi_3'(1), \quad \psi_1'''(\lambda_1) = \psi_2'''(\lambda_1), \quad \psi_2'''(\lambda_2) = \psi_3'''(\lambda_2),
\end{aligned} \tag{4}$$

where $\zeta = x/L$, F=PL^2/EI, $\alpha = \omega L^2\sqrt{m/EI}$, and the ratio of the non-dimensional foundation modulus and flexural rigidity k = $K\,L^2/(E\,I/L^2)$ characterizes the relative foundation stiffness. For distinct roots $\{n_1, n_2, n_3, n_4\}$ and $\{m_1, m_2, m_3, m_4\}$ of the characteristic polynomials $n^4 + Fn^2 - \alpha^2 = 0$ and $m^4 + Fm^2 - (\alpha^2 - k) = 0$ the d th derivative (including d=0) of solutions to Eq. (3) are

$$\begin{aligned}
&\psi_1^{(d)}(\zeta) = \sum_{i=1}^{4} C_{1,i} n_i^d e^{n_i\zeta} \quad \text{for } 0 < \zeta < \lambda_1,\\
&\psi_2^{(d)}(\zeta) = \sum_{i=1}^{4} C_{2,i} m_i^d e^{m_i\zeta} \quad \text{for } \lambda_1 < \zeta < \lambda_2,\\
&\psi_3^{(d)}(\zeta) = \sum_{i=1}^{4} C_{3,i} n_i^d e^{n_i\zeta} \quad \text{for } \lambda_2 < \zeta < 1.
\end{aligned} \tag{5}$$

The wide applicability of these explicitly complex solutions (valid provided $\alpha \neq 0$, $\alpha^2 - k \neq 0$, $F^2 + 4\alpha^2 \neq 0$, and $F^2 + 4(\alpha^2 - k) \neq 0$) outweighs any benefit from avoiding complex arithmetic by rewriting complex-exponentials as explicitly real combinations of trigonometric and exponential functions. Special cases with repeated roots are easily handled e.g. for

divergence ($\alpha=0$) $n^4+F\,n^2=0$ has roots $\{n_1,n_2,0,0\}$ and the solution is

$$\psi_1(\zeta)=C_{1,1}e^{n_1\zeta}+C_{1,2}e^{n_2\zeta}+C_{1,3}1+C_{1,4}\zeta,\quad 0<\zeta<\lambda_1,$$

$$\psi_2(\zeta)=C_{2,1}e^{m_1\zeta}+C_{2,2}e^{m_2\zeta}+C_{2,3}e^{m_3\zeta}+C_{2,4}e^{m_4\zeta},\quad \lambda_1<\zeta<\lambda_2,$$

$$\psi_3(\zeta)=C_{3,1}e^{n_1\zeta}+C_{3,2}e^{n_2\zeta}+C_{3,3}1+C_{3,4}\zeta,\quad \lambda_2<\zeta<1.$$

3. Matrix formulation

We describe only the generic case: the non-generic cases (we needed $\alpha=0$ and $\alpha^2-k=0$) are similar. Substituting the solution given by expression equation (5) into the 12 boundary and continuity conditions Eq. (4) gives the matrix equation

$$\mathbf{MC}=\mathbf{0}_{12,1} \tag{6}$$

for the complex twelve vector $\mathbf{C}=\{C_{1,1},\ldots C_{1,4},\ldots C_{3,1},\ldots C_{3,4}\}$ where $\mathbf{0}_{p,q}$ is the $p\times q$ zero matrix; **BI** is the 2×4 matrix with $\mathbf{BI}_{1,q}=1$ and $\mathbf{BI}_{2,q}=n_q$; **g0**, **g1**, **FF1**, and **FF2** are 1×4 matrices with **g0** = **FF2** + F **FF1** and **g1** = F **FF1** where $\mathbf{FF1}_{1,q}=e^{n_q}n_q^1$ and $\mathbf{FF2}_{1,q}=e^{n_q}n_q^2$; **CCn**($\lambda$) and **CCm**($\lambda$) are 4×4 matrices with $\mathbf{CCn}(\lambda)_{p,q}=e^{n_q\lambda}n_q^{p-1}$ and $\mathbf{CCm}(\lambda)_{p,q}=e^{m_q\lambda}m_q^{p-1}$; and finally **M** is a 12×12 matrix with $\mathbf{M}=\mathbf{M0}+\eta\mathbf{M1}$ where (for i=0 and 1) the block structure of **M0** and **M1** is

$$\mathbf{Mi}=\begin{pmatrix}\mathbf{BI} & \mathbf{0}_{2,4} & \mathbf{0}_{2,4}\\ \mathbf{CCn}(\lambda_1) & -\mathbf{CCm}(\lambda_1) & \mathbf{0}_{4,4}\\ \mathbf{0}_{4,4} & -\mathbf{CCm}(\lambda_2) & \mathbf{CCn}(\lambda_2)\\ \mathbf{0}_{1,4} & \mathbf{0}_{1,4} & \mathbf{FF2}\\ \mathbf{0}_{1,4} & \mathbf{0}_{1,4} & \mathbf{gi}\end{pmatrix}. \tag{7}$$

Three special cases (no foundation $\lambda_1=\lambda_2$; foundation extending from the built-in end $\lambda_1=0$; and foundation extending to the free end $\lambda_2=1$) can be computed without difficulty using the same formulation.

4. Analysis

The matrices **M0** and **M1** defined in Eq. (7) depend on the non-dimensional load F, foundation parameter k, foundation interval (λ_1,λ_2), and frequency α. Non-trivial solutions of Eq. (6), which exist if and only if Det(**M**)=0, give non-trivial displacements w indicating instability of w=0. Row linearity of the determinant gives $\mathrm{Det}(\mathbf{M})=\Gamma 0+\eta\Gamma 1$ where $\Gamma 0=\mathrm{Det}(\mathbf{M0})$ and $\Gamma 1=\mathrm{Det}(\mathbf{M1})$. This linearity in η allows us to complete an exhaustive analytical parameter study of the underlying physical problem. Rather than solving

$$\Gamma 0(F,k,\lambda_1,\lambda_2,\alpha)+\eta\,\Gamma 1(F,k,\lambda_1,\lambda_2,\alpha)=0 \tag{8}$$

directly for η we compute the determinants $\Gamma 0$ and $\Gamma 1$ separately to avoid difficulties associated with the singularity $\Gamma 1=0$.

For given F, k, λ_1, and λ_2 the non-dimensionalized frequency $\alpha=\omega L^2\sqrt{m/EI}$ gives the time dependence $e^{i\omega t}$ of the mode with follower parameter given by Eq. (8): $\alpha=0$ gives a non-trivial, static equilibrium; $\alpha>0$ gives a non-trivial, time-periodic mode.

4.1. Divergence critical loads

Non-trivial, static equilibria indicate a divergence instability. Values of the non-dimensional load F satisfying Eq. (8) with $\alpha=0$ (for a given non-dimensional foundation modulus k, foundation interval $0\le\lambda_1\le\lambda_2\le 1$, and follower parameter η) are divergence loads. The smallest divergence load for a given set of parameters is the critical divergence load.

Values of $\Gamma 0$ and $\Gamma 1$ with $\alpha=0$ (for k=10,100,200,400) are compiled on an extensive regular grid of F, λ_1, and λ_2 values with $0\le\lambda_1\le\lambda_2\le 1$, and $0\le F\le 50$. Divergence load curves are zero contours of $\Gamma 0+\eta\Gamma 1$ for fixed $a=(\lambda_2-\lambda_1)$, $b=0.5(\lambda_1+\lambda_2)$, and k as a function of η and F. Non-dimensionalized loads F on the lower branches of divergence load curves are critical divergence loads.

4.2. Flutter critical loads

Non-trivial, time-periodic modes indicate an incipient flutter instability. Values of the non-dimensional load F satisfying Eq. (8) with $\alpha>0$ (for a given non-dimensional foundation modulus k, foundation interval $0\le\lambda_1\le\lambda_2\le 1$, and follower parameter η) give non-trivial, time-periodic modes: the minimum of such F over all non-dimensional frequencies $\alpha>0$ is the critical flutter load.

We temporarily fix (and suppress the dependence on) k,λ_1,λ_2 and η to examine the dependence on α of loads $F_m(\alpha)$ which give non-trivial, time-periodic modes. Such loads satisfy Eq. (8) with $F=F_m(\alpha)$ which gives (with partial derivatives

evaluated at $F_m(\alpha)$, k, λ_1, λ_2 and α)

$$\left(\frac{\partial \Gamma 0}{\partial F}+\eta\frac{\partial \Gamma 1}{\partial F}\right)F'_m(\alpha)+\left(\frac{\partial \Gamma 0}{\partial \alpha}+\eta\frac{\partial \Gamma 1}{\partial \alpha}\right)=0,$$

when differentiated with respect to α. Combining this and the consequences ($\Gamma 0+\eta\Gamma 1=0$ and $F'_m(\alpha)=0$) of the critical flutter load definition gives the explicit $\eta-$independent flutter condition $\Gamma 1(\partial\Gamma 0/\partial\alpha)-\Gamma 0(\partial\Gamma 1/\partial\alpha)=0$.

Values of $\Gamma 0$ and $\Gamma 1$ (for k=10,100,200,400) are compiled on an extensive, regular grid of F, λ_1, λ_2, and α values with $0\le\lambda_1<\lambda_2\le 1$, $0\le F\le 50$, and $0\le\alpha\le 100$. Zero contours of $\Gamma 1(\partial\Gamma 0/\partial\alpha)-\Gamma 0(\partial\Gamma 1/\partial\alpha)=0$ (with differencing in α to compute accurate partial derivatives) as a function of α and F give critical flutter loads as a function of a, b, and k. Finally, the η values are back computed using cubic interpolation of the tabulated data for $\Gamma 0$ and $\Gamma 1$. Some care has to be taken when flutter loads cross the singular curves $\Gamma 1=0$.

4.3. Computational issues

4.3.1. Explicitly complex arithmetic

The only drawback of the explicitly complex computation is that incomplete floating point cancellation commonly leaves insignificant imaginary residues in computed results. $\Gamma 0$ and $\Gamma 1$ are normalized (only the ratio is significant) to be real and insignificant (in the computations reported less than 10^{-14}) complex residues simply neglected.

4.3.2. Computational range

Linearity in η is exploited (to avoid solving for F) by treating F as an input variable. As a consequence, the computational range of F is restricted. Throughout this study, the maximum non-dimensionalized load is 50. This is not an issue, because throughout the parameter ranges considered critical divergence loads and/or critical flutter loads were less than 50. Similar considerations apply to the non-dimensional frequency α.

4.3.3. Computational resolution

Tables of values (for k=10, 100, 200, 400) were created for $\Gamma 0$ and $\Gamma 1$ as functions of F, λ_1, λ_2, and α. There are: 201 F values (equally spaced) between 0 and 50; 41 λ_1 (and λ_2) values (equally spaced) between 0 and 1; and 1001 α values (non-linearly scaled to enhance low frequency coverage) between 0 and 20. The resolution in F is better than 0.125 while the resolution in λ_1 and λ_2 (and hence a and b) is better than 0.0125.

5. Results

The computational results are a comprehensive examination of the complete physical follower-parameter range $0\le\eta\le 1$ for $0\le\lambda_1\le\lambda_2\le 1$ (equivalently $a/2\le b\le 1-a/2$ where $0\le a\le 1$) with a resolution of $\Delta\lambda=0.025$ for k=10, 100, 200, and 400. This section summarizes the results.

Fig. 2 illustrates the typical effect (in the figure the foundation extends for half the beam i.e. a=0.5 and k=100) of changing the foundation center b. As the foundation moves from the built-in end b=0.25 to the free end b=0.75: critical flutter loads are non-monotone; critical divergence loads increase; and the flutter interval ($\eta_{\min}$,1] where flutter is the governing load expands.

Fig. 3 illustrates the typical effect (in the figure the partial foundation is centered on the beam i.e. b=0.5 and k=100) of changing the foundation length a. As the foundation is reduced from a full foundation a=1 to a quarter foundation a=0.25: critical flutter loads are non-monotone; critical divergence loads decrease; and the flutter interval expands.

Fig. 4 illustrates the typical effect (in the figure b=0.5 and a=0.5) of increasing the foundation modulus k for a partial foundation. As the foundation modulus increases: critical flutter loads are non-monotone; critical divergence loads increase; and the flutter interval first expands then shrinks.

Fig. 5 shows the effect of increasing the foundation modulus k for a complete foundation i.e. a=1. As the foundation modulus increases: critical flutter loads do not change; critical divergence loads increase; and the flutter intervals expands to approximately (0.32,1] when $k\approx 50$ after which it is constant. Note, stiff foundations ($k>100$) and any significant follower component ($\eta>0.33$) are very susceptible to flutter instability. Fig. 5 recreates discrete values for ($\eta=0.1$, 0.2, …, 0.9, 1.0) from Rao and Rao [13] and the lower k values reported in Fig. 2 of Kirillov and Seyaranien [14]. The classic text Heténi [26] analyzes the loading beneath an aqueduct by considering a 0.3 m thick concrete beam (with elastic modulus 17 GPa) supported by a soil with foundation modulus 45 MPa m^{-1}. For this example, k=10, 100, and 400 correspond to beams of length 1.7, 3.0, and 4.3 m, respectively.

We now focus on the variation of the critical flutter load as a function of the location and size of the foundation for various values of the follower parameter. Fig. 6 shows the percentage deviation of the critical flutter load (from the fully supported critical flutter load—which is of course equal to the unsupported flutter load by Smith and Herrmann [9]) as a function of a and b in the fully tangential case ($\eta=1$) for k=100. The parameter region is triangular since $a/2<b<1-a/2$. The foundation can increase the critical flutter load (over a 19 percent increase for a 15 percent foundation extending from

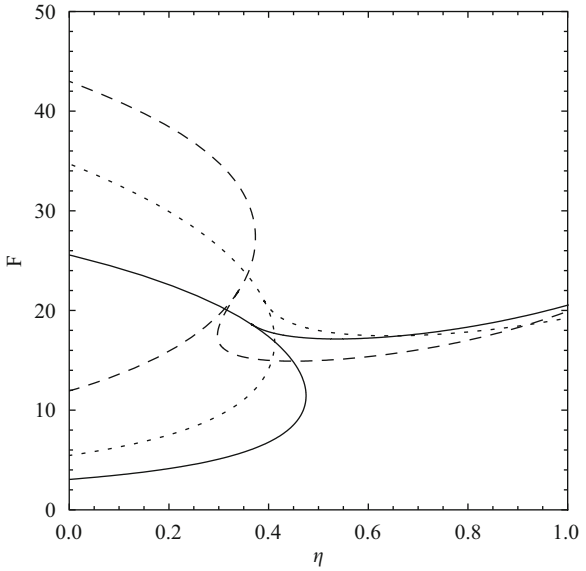

Fig. 2. Divergence (low values of η) and flutter (high values of η) critical loads for $k=100$ and a=0.5: The solid curves are b=0.25; the dotted curves are b=0.5; and the dashed curves are b=0.75.

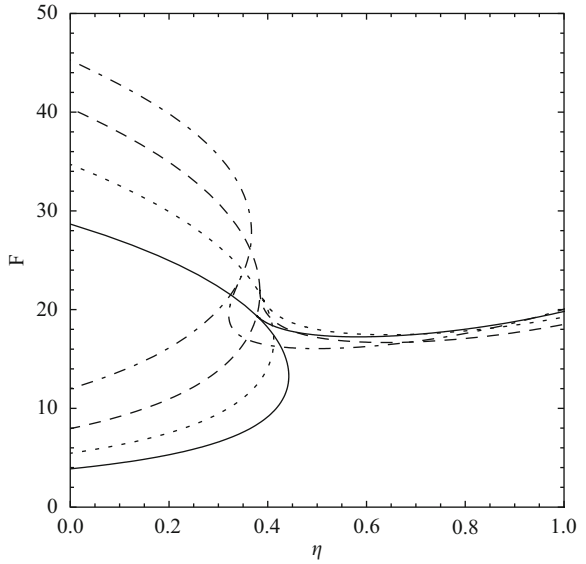

Fig. 3. Divergence (low values of η) and flutter (high values of η) critical loads for k=100 and b=0.5: The solid curves are a=0.25; the dotted curves are a=0.5; the dashed curves are a=0.75; and the dot-dashed curves are a=1.00.

the free end i.e. a=0.15 and b=0.925) or decrease the critical flutter load (over an 11 percent decrease for a 35 percent foundation approximately 70 percent of the way out from the built-in end i.e. a=0.35 and b=0.70). Zero contours indicate where the foundation has no effect on the critical flutter load separating parameters which stabilize the column by increasing the flutter load from those that destabilize the column. Zero contours leave the a=0 border at $b\approx 0.45$ and 0.85. In other words, for $\eta=1$ and k=100 a short foundation is destabilizing for $0.45<b<0.85$ and stabilizing otherwise. The contours are closest together adjacent to the $b=1-a/2$ border indicating that the flutter load is most sensitive to the 5–10 percent of the foundation nearest the free-end. In this region, contours are essentially parallel to the border indicating that in this region the critical flutter load essentially depends only on $b+a/2$ with the consequence that the critical flutter load increases approximately twice as fast in b as it does in a.

Our computed critical flutter load for $\eta=1$ is independent of k when a=1.0, as expected. The value of 21.01 is well within 0.125 (the numerical resolution) of the accurate value of 21.051. It is significantly better than the approximate value 21.6462 reported in Eliashakoff and Wang [17].

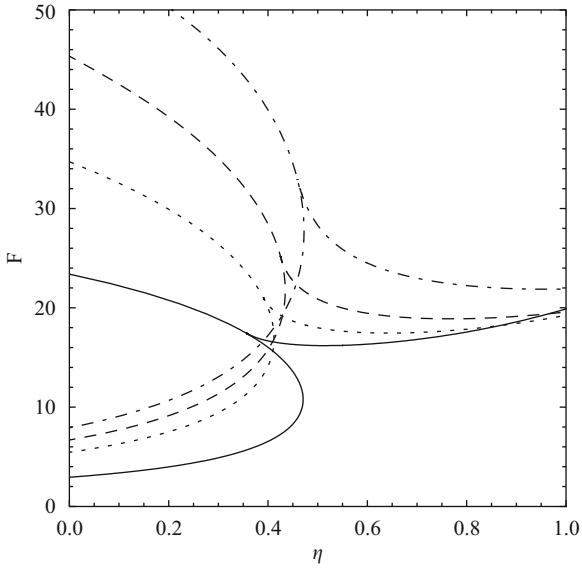

Fig. 4. Divergence (low values of η) and flutter (high values of η) critical loads for a=0.5 and b=0.5. The solid curves are k=10; the dotted curves are k=100; the dashed curves are k=200; and the dot dashed curves are k=400.

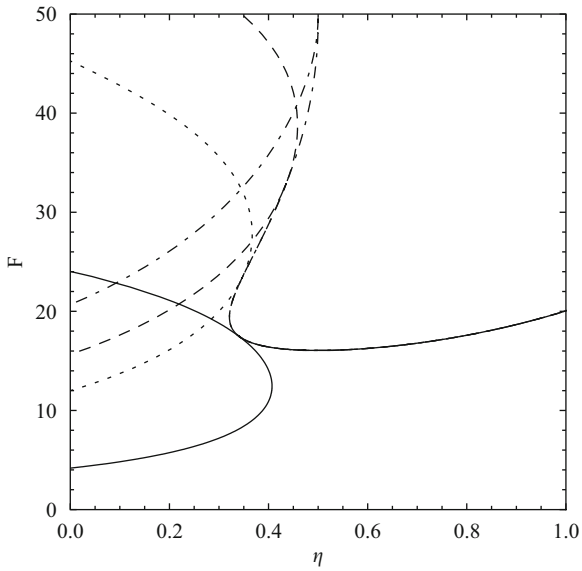

Fig. 5. Divergence (low values of η) and flutter (high values of η) critical loads for a=1.0 and b=0.5. The solid curves are k=10; the dotted curves are k=100; the dashed curves are k=200; and the dot dashed curves are k=400. Note, as expected for a complete foundation all the flutter curves superimpose because the flutter load is independent of k.

Fig. 7 shows the percent deviation of the critical flutter loads from the fully supported foundation as a function of a and b for $\eta = 0.6$ and k=100. The foundation can again increase or decrease the flutter load (over a 7 percent increase for a 65 percent foundation extending from the built-in end, i.e. a=0.65 and b=0.325 and over a 7 percent decrease for a 30 percent foundation approximately 75 percent of the way out from the built-in end, i.e. a=0.30 and b=0.75) depending on the length a and center b of the foundation. It is noteworthy that the easily explained peak for $\eta = 1$ with a foundation concentrated at the free-end has almost completely vanished for $\eta = 0.6$. As a general principle, both the increase and decrease are smaller than in the pure tangential case shown in Fig. 6.

The side b=a/2 i.e. $\lambda_1 = 0$ and $\lambda_2 = a$ of Fig. 6 is an exact computation of the approximate results in Eliashakoff and Wang [17]: their two-term Galerkin approximation is easily modified (literally replacing the unit-step function $U[a-y]$ with

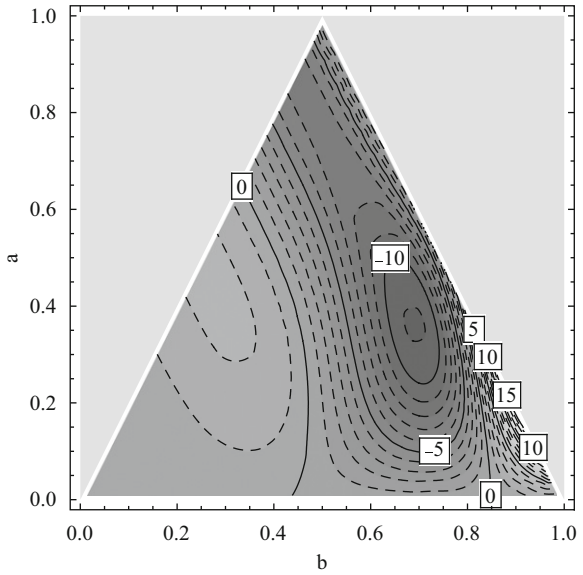

Fig. 6. Percentage deviation of normalized flutter critical loads for k=100 and $\eta = 1$. Solid contours are multiples of 5 percent.

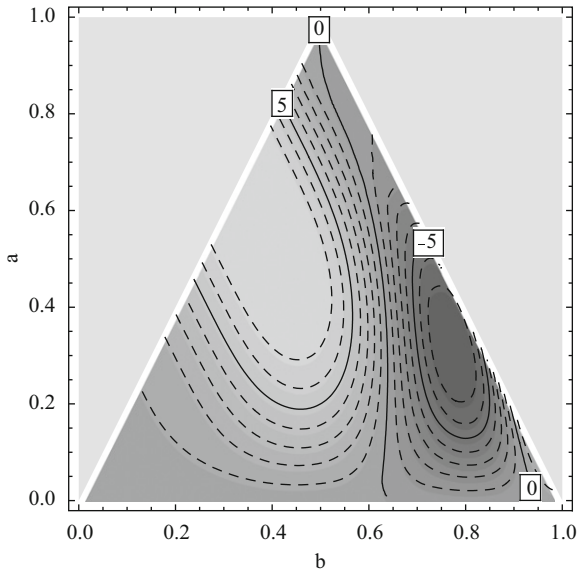

Fig. 7. Percentage deviation of normalized critical flutter loads for k=100 and $\eta = 0.6$. Solid contours are multiples of 5 percent.

$U[y-a]$) to compute the second sloping side b=$1-a/2$ i.e. $\lambda_1 = 1-a$ and $\lambda_2 = 1$ in Fig. 6. Fig. 8 shows the approximate normalized critical flutter loads computed using the technique described in [17].

Our analytical results in Fig. 6 qualitatively match (along the two sloped edges of the triangle) the two-term Galerkin numerical approximations in Fig. 8. The recomputation and extension of [17] shown in Fig. 8 was prompted by the fact that Fig. 6 (along the sloped side b=$a/2$ of the triangle) does not match the approximate results in [17]. Having verified our results with the their approximation we now believe that there is a typographical error in the algebraically involved computation in [17].

6. Conclusions

Making the foundation stiffer (by increasing k), extending the foundation (by increasing a), or moving the foundation towards the free-end (by increasing b) all stabilize the beam against divergence by increasing the critical divergence load.

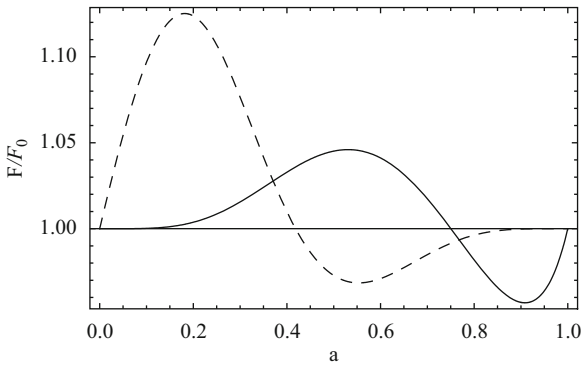

Fig. 8. Elishakoff and Wang [17] approximation, normalized (by the no foundation load F_0) flutter critical loads for $k=100$ and $\eta=1$. The dashed curve is a foundation extending from the free–free end i.e. ($b=1-a/2$). The solid curve is a foundation extending from the built-in end, i.e. $b=a/2$.

Extending the foundation or moving the foundation towards the free-end of the beam decreases the range of η values for which divergence is the governing failure mode. As in Ref. [14], stiffening the foundation can either increase or decrease the range of η values for which divergence is the governing failure mode.

The critical flutter load depends in a complicated manner on η, k, a, and b. In general: the effects on the critical flutter load is less pronounced for intermediate values of η than for fully follower loads; for a partial foundation near the free-end the critical flutter load increases with both a and b with the load approximately twice as sensitive to b as a.

For a fully supported beam ($a=1$ and $b=0.5$) the critical flutter load is independent of k and for stiff foundations ($k \geq 100$) with moderately follower loads ($\eta > 0.32$) the governing mode is flutter. As a result, the governing load for a fully supported beam is independent of k for $k \geq 100$ and $\eta > 0.32$.

Acknowledgements

We would like to acknowledge the anonymous referee who provided a useful reference and improved the readability of the article.

References

[1] S.P. Timoshenko, J.M. Gere, *Theory of Elastic Stability*, McGraw-Hill, New York, 1961.
[2] D.O. Brush, B.O. Almarotto, *Buckling of Bars, Plates, and Shells*, McGraw-Hill, New York, 1975.
[3] G.J. Simitses, *An Introduction to the Stability of Structures*, Prentice-Hall, New Jersey, 1976.
[4] N.S. Astapov, A.G. Demeshkin, V.M. Kornov, Buckling of a bar on an elastic base, *Journal of Applied Mechanics and Technical Physics* 35 (1994) 739–744.
[5] A.R. Toakley, Buckling loads for elastically supported struts, *Journal of Engineering Mechanics Division ASCE* 91 (1965) 205–231.
[6] K.L. Lee, Buckling of partially embedded piles in sand, *Journal of Soil Mechanics and Foundations Division ASCE* 94 (1968) 255–270.
[7] A. Siva Reddy, A.J. Valsangkar, Buckling of fully and partially embedded piles, *Journal of the Soil Mechanics and Foundations Division ASCE* 96 (1970) 1951–1965.
[8] B.B. Budkowska, C. Szymczak, Partially embedded piles subjected to critical buckling load—sensitivity analysis, *Computers and Structures* 61 (1996) 193–196.
[9] T.E. Smith, G. Herrmann, Stability of a beam on an elastic foundation subjected to a follower force, *Journal of Applied Mechanics ASME* 39 (1972) 628–629.
[10] C. Sundarajan, Stability of columns on elastic foundations subjected to conservative and non-conservative forces, *Journal of Sound and Vibration* 37 (1974) 79–85.
[11] A. Jacoby, I. Elishakoff, Discrete-continuous elastic foundation may leave the flutter load of the pflüger column unaffected, *Journal of Sound and Vibration* 108 (1986) 523–525.
[12] I. Elishakoff, A. Jacoby, Influence of various types of elastic foundation on the divergence and flutter of Ziegler's model structure, *Journal of Applied Mathematics and Physics* 38 (1987) 779–784.
[13] B. Nageswara Rao, G. Venkateswara Rao, Stability of a cantilever column resting on an elastic foundation subjected to a subtangential follower force at its free end, *Journal of Sound and Vibration* 125 (1988) 570–577.
[14] O.N. Kirillov, A.P. Seyranian, Solution to the Herrmann–Smith problem, *Doklady Physics* 47 (2002) 767–771.
[15] W. Hauger, K. Vetter, Influence of an elastic foundation on the stability of a tangentially loaded column, *Journal of Sound and Vibration* 47 (1976) 296–299.
[16] S.Y. Lee, C.C. Yang, Non-conservative instability of non-uniform beams resting on an elastic foundation, *Journal of Sound and Vibration* 169 (1994) 433–444.
[17] I. Elishakoff, X. Wang, Generalization of Smith-Herrmann problem with the aid of computerized symbolic algebra, *Journal of Sound and Vibration* 117 (1987) 537–542.
[18] W.T. Koiter, Unrealistic follower forces, *Journal of Sound and Vibration* 194 (1996) 636–638.
[19] Y. Sugiyama, M.A. Langthjem, B.J. Ryu, Realistic follower forces, *Journal of Sound and Vibration* 225 (1999) 779–782.
[20] M.A. Langthjem, Y. Sugiyama, Dynamic stability of columns subjected to follower loads: a survey, *Journal of Sound and Vibration* 238 (2000) 809–851.
[21] M.K. Ramasubramanian, O.M. Barham, V. Swaminathan, Mechanics of a mosquito bite with applications to microneedle design, *Bioinspiration and Biomimetics* 3 (2008) #046001.
[22] T. Andriacchi, A. Schultz, T. Belytschko, J. Galante, A model for studies of mechanical interactions between the human spine and rib cage, *Journal of Biomechanics* 7 (1974) 497–507.

[23] A.G. Patwardhan, R.M. Havey, K.P. Meade, B. Lee, B. Dunlap, A follower load increases the load-carrying capacity of the lumbar spine in compression, *Spine* 24 (1999) 1003–1009.
[24] K. Kim, Y.H. Kim, S.K. Lee, Increase of load-carrying capacity under follower load generated by trunk muscles in lumbar spine, *Proceedings of the Institution of Mechanical Engineers, Part H: Journal of Engineering in Medicine* 221 (2007) 229–235.
[25] G. Jayaraman, A. Struthers, Divergence and flutter instability of elastic specially orthotropic plates subject to follower forces, *Journal of Sound and Vibration* 281 (2005) 357–373.
[26] M. Hetényi, *Beams on Elastic foundation: Theory with Applications in the Fields of Civil and Mechanical Engineering*, University of Michigan Press, Ann Arbor, USA, 1946.